

Synthesis, Characterization, Magnetic and Photocatalytic properties of Bi, Co and Mn Co-doped Neodymium Ferrite ($\text{Nd}_{0.5}\text{Bi}_{0.2}(\text{Co}_{0.2}\text{Mn}_{0.1})\text{FeO}_{(3-\delta)}$) Solid Solution

*Ibrahim Abdulkadir,¹Bice S. Martincigh and ¹Sreekantha B. Jonnalagadda

Department of Chemistry, Ahmadu Bello University, Sokoto Expressway, Samaru, Zaria-Nigeria,

¹School of Chemistry and Physics, University of KwaZulu-Natal, Westville Campus, Private Bag X54001, Durban 4000, South Africa

Corresponding Author: ibrahim.abdulkadir@gmail.com.

Abstract

Bismuth and cobalt co-doped perovskite-type nanomaterials with the composition $\text{Nd}_{0.5}\text{Bi}_{0.2}(\text{Co}_{0.3}\text{Mn}_{0.1})\text{FeO}_{3-\delta}$ were synthesized by using the citric acid sol-gel route and annealed at annealing temperatures (T_A) of 400, 750 and 900°C to produce powders labelled NdCo400, NdCo750 and NdCo900 respectively. The powders obtained were characterized using Powder X-ray diffraction (PXRD) analysis, transmission electron microscopy (TEM), Fourier transform infrared spectroscopy (FTIR), Brauner-Emmet-Teller (BET) Method, vibrating sample magnetometer, (VSM) and photoluminescence spectroscopy (PL). The powder X-ray diffraction (PXRD) analysis of the powders showed that they contain highly crystalline orthorhombic perovskite-type nanoparticles whose crystallinity increased with higher annealing temperature. The lattice parameters, after refinement for NdCo900, showed that the parameters a, b and c have values 5.939, 5.488 and 7.740 Å respectively. The TEM results showed cubic crystallites with average crystalline size within the range of 17-30 nm for both NdCo750 and NdCo900 respectively. The BET specific surface areas obtained was 12.46 and 5.92 $\text{m}^2 \text{g}^{-1}$ for NdCo750 and NdCo900. Room temperature VSM analysis showed T_A dependent properties for the powders NdCo400 (11.09 emu g^{-1} , 402 Oe), NdCo750 (9.00 emu g^{-1} , 2181 Oe) and NdCo900 (9.44 emu g^{-1} , 683.16 Oe) for saturation magnetization M_S and coercive field H_C values respectively. Photoluminescence spectroscopy showed that the powders were all active in the visible region and could be useful for visible light photodegradation of organic dyes. NdCo900 was the most effective for the decolourization of RhB dye with $k_{\text{obs}} = 1.6 \times 10^{-2} \text{ min}^{-1}$ and percent efficiency $E\% = 99.1\%$. A 73% mineralization of the dye was also achieved after 3 h.

Keywords: Perovskites, Coercive field, Photoluminescence, Photocatalytic activities.

1. INTRODUCTION

Perovskites are a group of materials that can generally be represented by the formula ABX_3 (where A^{3+} could be a large rare-earth metal, B^{3+} is a smaller transition metal and X^{2-} is a non-metal, mostly, oxygen). The perovskite structure is flexible and can accommodate almost all the elements in the periodic table. Their tendency to display an array of very interesting properties have made them the focus of numerous scientific studies.

Perovskites and perovskite-like multiferroic nanomaterials have potentials for application in a variety of crucial advanced technologies. They have been subjected to intensive investigation due to their potential for use as cathodes in solid oxide fuel cell (SOFC) (Maguire *et al.*, 2000; Skinner, 2001; Inprasit *et al.*, 2016; Lerdprom *et al.*, 2017) sensors (Lantto *et al.*, 2004; Ghasdi *et al.*, 2011), piezo- and pyroelectric, acoustic transducers (Paik *et al.*, 1999; Peel *et al.*, 2013; Ramajo *et al.*, 2014), capacitors and memory devices (Chung *et al.*, 2008), as well as catalytic and Photocatalytic materials (Machida *et al.*, 2000; Tang *et al.*, 2007; Kanhere *et al.*, 2012; Yu *et al.*, 2012; Zhu *et*

al., 2014). For nanomaterials, the synthesis route has been shown to impact on the size and morphology as well as the surface area of the particles of the synthesized material and hence its properties. For perovskites and perovskite-like oxides, the annealing temperature for making the finished material is usually high and this leads to materials with large particle sizes and very low surface area, which is not good for photocatalysis (Zhu *et al.*, 2014) for example, the optical and magnetic properties of these materials may also be affected. Annealing environment may also play a role in determining the properties of semiconductor stable solid solution materials tailored towards specific functions have been made by selecting elements of suitable properties as dopants.

The electrical, visible light Photocatalytic as well as weak ferromagnetic properties of perovskites can be manipulated/enhanced by introducing lone pair bearing transition metals (e.g. Bi^{3+} , Pb^{3+}) (Khomskii, 2006) and divalent alkaline earth metal dopants (Ca^{2+} , Sr^{2+} and Ba^{2+} to create distortions or oxygen deficiency in the lattice of the material due to bond length variation (Lu

et al., 2005; Zhang *et al.* 2008) on the A and/or B site by a simple synthesis method. In this work, we report the synthesis of a substituted orthoferrite $\text{Nd}_{0.5}\text{Bi}_{0.2}\text{Co}_{0.2}\text{Mn}_{0.1}\text{FeO}_3$ via a simple pechini-type citric acid synthesis. The major aim in this work is to study the magnetic as well as the Photocatalytic properties of this substituted ferrite and the effect of annealing temperature (at 400°C, 750°C and 900°C) on its properties.

2. MATERIALS AND METHODS

Nd_2O_3 (99.8%), citric acid (99.7%) (BDH Chemicals), $\text{Fe}(\text{NO}_3)_3 \cdot 9\text{H}_2\text{O}$ (98%), $\text{Bi}(\text{NO}_3)_3 \cdot 5\text{H}_2\text{O}$ (97%), $\text{Co}(\text{NO}_3)_2$ (99%) $\text{Mn}(\text{CH}_3\text{OO})_2$ (99 %), concentrated HNO_3 (55%), ethylene glycol (99%) (Promark Reagents), rhodamine B (The Coleman and Bell Co., U.S.A.) and H_2O_2 30% vol. (100 vol) (Minema Chemicals) were used as received. Deionised water from a Millipore Milli-Q Elix 5 UV system was used throughout and is hereafter referred to as Milli-Q water.

2.1 Synthesis of $(\text{Nd}_{0.5}\text{Bi}_{0.2}\text{Co}_{0.2}\text{Mn}_{0.1})\text{FeO}_{(3-\delta)}$

$(\text{Nd}_{0.5}\text{Bi}_{0.2}\text{Co}_{0.2}\text{Mn}_{0.1})\text{FeO}_{(3-\delta)}$ samples were prepared by a citric acid sol-gel process. $\text{Fe}(\text{NO}_3)_3 \cdot 9\text{H}_2\text{O}$ (0.03 mol) was dissolved in Milli-Q water (20.00 cm^3). Nd_2O_3 (0.0075 mol), $\text{Co}(\text{NO}_3)_2$ (0.006 mol) $\text{Mn}(\text{CH}_3\text{OO})_2$ (0.003 mol) and $\text{Bi}(\text{NO}_3)_3 \cdot 5\text{H}_2\text{O}$ (0.006 mol) were dissolved in dilute nitric acid (about 15 cm^3 , 6 mol dm^{-3}) solution to give the amount of metals required to fulfil the material's stoichiometry. The two solutions were mixed thoroughly, made up to 200 cm^3 with water (Milli-Q) and then gradually poured into a burette. The solution was then added (drop-wise) to a citric acid solution (400 cm^3 , 0.15 mol) in a beaker which was continuously stirred by magnetic stirrer at room temperature to form a clear solution. Once the addition was completed and still stirring, the temperature of the mixture was raised to 90°C and allowed to stand until the volume of the solution was reduced to about 50 cm^3 , ethylene glycol (100 cm^3) was added and the heating and stirring continued until a thick gel was formed. The gel was then removed from the beaker and placed in a crucible in an oven at a temperature of 120°C for 24 hrs to dry. The dry gel was subsequently pre-calcined at 400°C for 4 hrs to remove all the organic components. A separate sample portions of the pre-calcined dry gel were subsequently annealed in a muffle furnace for 4 h at annealing temperatures (T_A) of 750 and 900°C respectively. A dry brown powder of the material $\text{Nd}_{0.5}\text{Bi}_{0.2}(\text{Co}_{0.2}\text{Mn}_{0.1})\text{FeO}_{(3-\delta)}$ was obtained after the precalcination process. The colour of the powders changed gradually from brown to black as the annealing temperature increased. The samples were labelled NdCo followed by the temperature at which they were annealed (NdCo400, NdCo750 and

NdCo900 for samples annealed at 400, 750 and 900°C respectively).

2.2 Characterisation

Transmission electron microscopy (TEM) micrographs of the samples were collected on a JEOL JEM 1010 instrument (Tokyo, Japan). Scanning electron microscopy (SEM) data were also collected on a ZEISS Ultra plus field emission gun scanning electron microscope for the analysis of the morphology of the crystals. The crystals lattice structures were determined by powder X-ray diffraction (PXRD) analysis by using a Bruker Advance D8 diffractometer equipped with a XRK 900 reaction chamber, a TCU 750 temperature control unit and a Cu K_α radiation source ($\lambda = 1.5406 \text{ \AA}$). The scan step was set at 0.02° and a rotation speed of 15 RPM. The scanning was done from 2 θ values of 10°C to 90°C. Crystallite sizes (D) were calculated by using the Scherrer equation, $D = k\lambda/\beta\cos\theta$ (where k is the Scherrer constant, λ is the wavelength of the radiation and β is the full width at half maximum). The Specific surface areas were determined by nitrogen adsorption and BET equation method with a Micromeritics Tristar II 3020 fully automated three station surface area while the pore sizes were determined by using porosity analyser. The magnetic properties were analysed by using a LakeShore model 735 vibrating sample magnetometer (VSM) which had been calibrated with a standard Ni sphere of saturation magnetization 54.7 emu g^{-1} .

The maximum applied magnetic field was 14 kOe and analyses were done at room temperature. Surface characterisation of the powders was carried out on a Perkin Elmer FTIR Spectrum 100 spectrometer fitted with an attenuated total reflectance (ATR) accessory and bands were scanned from 350 to 4000 cm^{-1} value. The photoluminescence spectra were monitored at two excitation wavelengths (390 and 400 nm) by means of a Perkin Elmer LS 55 spectrofluorimeter equipped with a high energy pulsed xenon source for excitation.

2.3 Photocatalytic screening

The Photocatalytic activity of each sample was tested on Rhodamine B dye in the absence and presence of H_2O_2 at room temperature. A 26 W fluorescent lamp (Osram Dulux D, 26 W, 1800 lm) placed in a quartz jacket and held at about 7 cm above the RhB dye solution (which was continuously being stirred with a magnetic stirrer) was used for the irradiation. The system contained 1.5 g dm^{-3} of synthesized materials and H_2O_2 ($3.0 \times 10^{-5} \text{ mol dm}^{-3}$). A period of 30 min was allowed for equilibration in the dark before the lamp was turned on. Aliquots of the dye solution were withdrawn at intervals of 20 min to monitor the photodegradation process by measuring the absorbance of the withdrawn aliquot at a λ_{max} of 556 nm on a Biochrom Libra S6 UV

spectrophotometer. The extent of mineralization was also investigated by determining the chemical oxygen demand (COD) of the degraded solution after 180 min of degradation activity by means of standard method as described in the literature (Williams, 2001).

3. RESULTS AND DISCUSSION

The results obtained from characterisation of the powders are presented and discussed in this subsection.

3.1 Crystal Phase Characterization

The PXRD diffractograms of the samples prepared at annealing temperatures (T_A) of 400°C, 750°C and 900°C are shown in Figure 1. The perovskite peaks can be seen growing at $T_A = 400^\circ\text{C}$. This indicates the nucleation and growth of the perovskite phase may have started at a lower temperature. Peaks corresponding to the 101, 111, 200, 121, 202 and 042

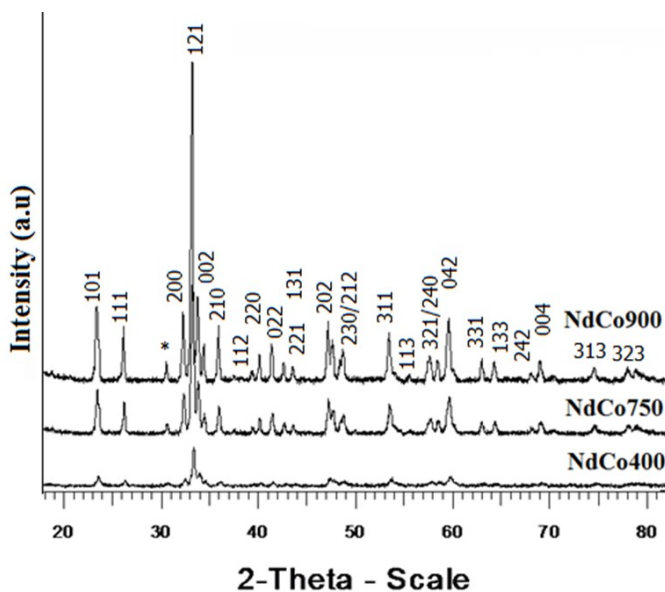


Figure 1. Powder X-ray diffractograms for the powders showing the evolution of the perovskite peaks as the annealing temperatures increased from 400 to 900°C

orthorhombic planes can be clearly identified in the diffractogram at $T_A = 400^\circ\text{C}$, but the presence/absence of other peaks indicated that for this T_A , the powder may contain largely mixed oxides and even some amorphous materials. The perovskite peak intensities increase for higher T_A , indicating an increase in crystallinity and also an increase in the phase purity of the powders. The powders crystallized in an orthorhombic perovskite lattice at higher T_A (i.e. 750°C). Some researchers have also obtained the orthorhombic lattice for NdFeO_3 and Co-doped NdFeO_3 powders at 750°C and above using different synthesis methods (Nforna *et al.*, 2020; Shalini *et al.*, 2020; Nguyen *et al.*, 2021).

The presence of the peak at 2θ angle = 30 degrees (asterisked *) indicates that the ions may not have all been incorporated into the perovskite lattice or it may be an indication of the presence of a secondary phase. The broadening of the peaks is due to the nanoparticulate nature of the crystallites. A reduction in the broadening of the peaks for $T_A = 900^\circ\text{C}$, coupled with the increase in peak intensities indicate an increase in crystallite sizes which is confirmed by crystallite size values obtained by applying the Scherrer equation to the 121 planes (Table 1). Higher T_A , is therefore, accompanied by an increase in phase purity, crystallinity as well as crystallite sizes. Table 1 also shows the calculated lattice parameters obtained by using the *Diffracplus* software and matching the peaks with that of (NdFeO_3 (JCPDS, file no. 25-1149)). The cell volumes were only slightly affected by the change in T_A . A slight increase was observed in the cell volume between $T_A = 750$ and 900°C. This could be the point at which the ions are maximally incorporated into the perovskite lattice.

3.2 Morphology

Figure 2 shows the SEM micrographs for samples NdCo400, NdCo750 and NdCo900. The perovskite crystallites of size range below 10 can be seen clearly at $T_A = 400^\circ\text{C}$ (Figure 2a). This shows the initial stage of formation of the powder crystallites. The TEM for NdCo400 (Figure 2a Inset) also show crys-

Table 1: Variation in cell parameters and specific surface areas for samples annealed between 750 °C and 900°C, crystallite sizes were calculated from Scherrer equation.

Samples	Cell parameters				Lattice system	Crystallite sizes/ nm	SSA/m ² g ⁻¹ (± 0.01)
	a /Å	b /Å	c /Å	V /Å ³			
NdCo750	5.393	5.488	7.740	410.94	Orthorhombic	19.31	12.46
NdCo900	5.402	5.491	7.812	405.93	Orthorhombic	30.81	5.92

tallite sizes estimated to be below 10 nm in sizes. At $T_A = 750^\circ\text{C}$, the SEM micrograph shows that crystallites have grown in size relative to NdCo400 and spherical and cubic shaped perovskite crystallites can be seen from the TEM micrograph (Figure 2b Inset). The crystallite sizes estimated at this stage range between 13 and 17 nm. At 900°C the NdCo900 crystallites become even larger as can be observed from the SEM micrograph (Figure 2c) with crystallite sizes of about 26 nm estimated from the TEM (Figure 2c Inset). This agrees with the observation made from the PXRD data and calculation using Scherrer equation.

3.2 BET surface areas

Figure 3 shows the nitrogen adsorption-desorption isotherms for the powders. The isotherms conform to the type IV isotherm on the IUPAC scale (Sing *et al.*, 1985). The BET specific surface area obtained for both powders were $5.92\text{ m}^2\text{ g}^{-1}$ for NdCo900 and $12.46\text{ m}^2\text{ g}^{-1}$ for NdCo750 (Table 1). The presence of the hysteresis loop, which is related to capillary condensation at $T_A = 750^\circ\text{C}$ shows that crystallites contain some mesopores. At $T_A = 900^\circ\text{C}$ however, the P/P_0 is pushed much closer to 1 indicating a preponderance of macropores at higher T_A . The plot of pore area Vs pore diameter (inset in Figure 3) shows the pore size distribution of the powders. The pores are mostly mesopores at low T_A value. The sharpness of the peaks indicates a sort of uniformity or a narrow pore size distribution in the powders at $T_A = 750^\circ\text{C}$. At $T_A = 900^\circ\text{C}$ however, shows the presence of very few mesopores. The decrease in the mesopore areas and the increase in particle sizes is re-

sponsible for the decrease in the values of the specific surface areas of the powders.

3.4 Surface characterization

Figure 4 shows the Fourier transform infrared spectra of the samples collected between wavelengths 380- and 4000 cm^{-1} . The spectra show two important peaks, one at about 1400 cm^{-1} and the other at around 600 cm^{-1} . The peak at 1400 cm^{-1} is assigned to stretching vibrations of -OH groups from water molecules adsorbed on the surface of the crystals. The intensity of this peak decreases as T_A increases, indicating the removal of the

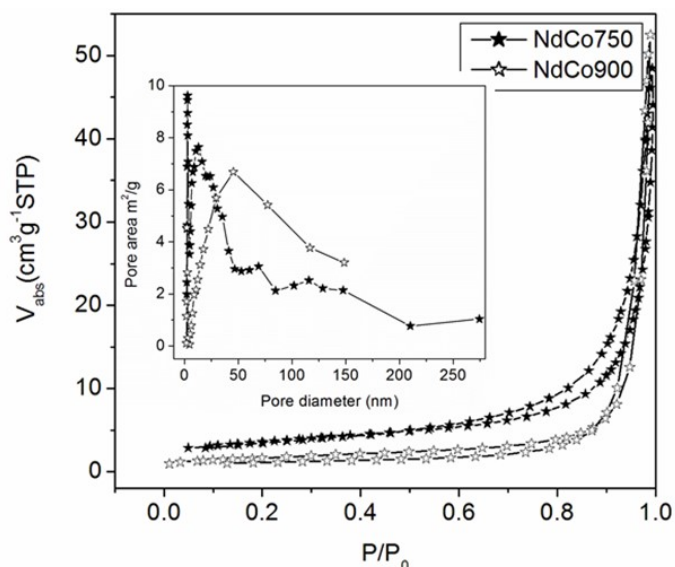


Figure 3. Adsorption-desorption isotherms for powders annealed at T_A 750 and 900°C . The inset shows the disappearance of modal mesopore peaks as T_A increased

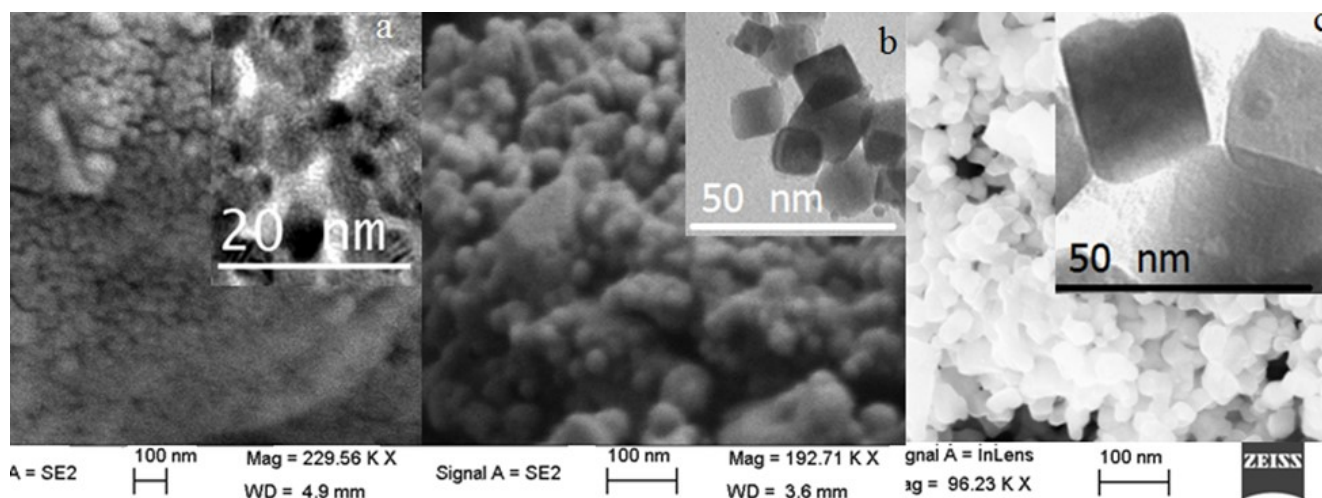


Figure 2. SEM micrographs with the corresponding TEM images (Inset) for (a) NdCo400, (b) NdCo750 and (c) NdCo900 showing the increase in crystallite size as T_A increases

water molecules at the surface of the material. It could also be an indication of a reduction in the surface area as T_A increases. The peak at 600 cm^{-1} is assigned to stretching modes for O-Fe bonds. This is an indication of the progress of the formation of the perovskite

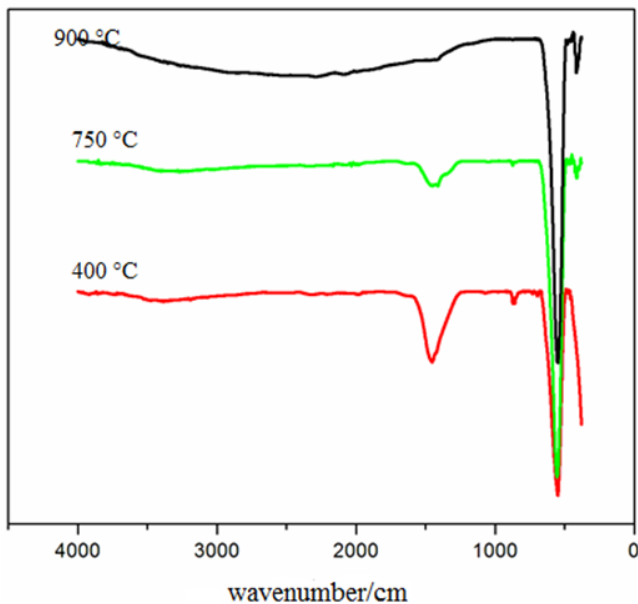


Figure 4. Fourier transform infrared spectra for NdCo400, NdCo750 and NdCo900 showing the reduction in peak intensity at 1400 cm^{-1} and an increase in peak intensity at 600 cm^{-1} with increase in annealing temperature.

lattice in agreement with the observation from the PXRD diffractograms.

3.5 Magnetic Properties

Perovskite solid solution ferrites have been reported to have antiferromagnetic properties due to the formation of bond overlaps between Fe ions and the p orbitals of oxygen ions which leads to the formation of $\text{Fe}^{3+}\text{-O-M}^{3+}$ bonds (where M^{3+} is Bi^{3+} , Fe^{3+} and Mn^{3+}). The introduction of an M^{2+} ion into the lattice would lead to a distortion in the bond angle of the Fe-O-Fe arrangement. Furthermore, the introduction of Co^{2+} into the lattice could either lead to the formation of Fe^{4+} in order to fulfil the requirements of charge compensation or result in the creation of oxygen vacancies and these contribute to the ferromagnetic characteristics (Liang *et al.*, 2005; Li *et al.*, 2007; Khomchenko *et al.*, 2008; Wang *et al.*, 2009). The result of the room temperature (RT) magnetization measurements of the powders is presented in Figure 5. The highest value of magnetization of 7.67 emu g^{-1} was obtained for NdCo400.

A general decrease in magnetization is observed for powders annealed at higher T_A . This decrease in M_S corresponds to the increase in crystallinity as can be seen from the PXRD (Figure 1). At $T_A = 400^\circ\text{C}$, the powders are composed mainly of mixed oxides. As the T_A is increased, more ions are incorporated into the perovskite lattice and Fe^{2+} ions are oxidized to Fe^{3+} in the perovskite octahedral site. This leads to the formation of more of the antiferromagnetic $\text{Fe}^{3+}\text{-O-M}^{3+}$ superexchange which results in a reduction in the value of M_S for NdCo750 and NdCo900. M_S values of 9.00 emu g^{-1} and 9.44 emu g^{-1} were obtained for NdCo750 and NdCo900 which are much higher than values of 0.98 emu g^{-1} obtained for Co doped NdFeO_3 by Nguyen *et al.*, (2021) and 0.87 emu g^{-1} obtained for Co doped NdFeO_3 by Nforna *et al.*, (2021).

The coercive fields (H_C) values showed a reverse trend compared to the M_S values. The H_C values increased sharply for NdCo750 and NdCo900 (Table 2). The highest H_C values were obtained for NdCo750 with a value of 2181 Oe which is much higher than the H_C value reported for NdFeO_3 by Nforna *et al.*, (2021). This increase in H_C can be attributed to the increase in sizes of the crystallites which is related to magnetocrystalline anisotropy (Herzer, 1990) as the crystallite sizes increased with T_A . Interactions between ferromagnetic and antiferromagnetic exchanges could also be a major contributor at this level, which will also be a confirmation of the presence of a secondary phase as observed from PXRD data. The squareness values (M_R/M_S) all remain low, indicating soft magnetic properties and do

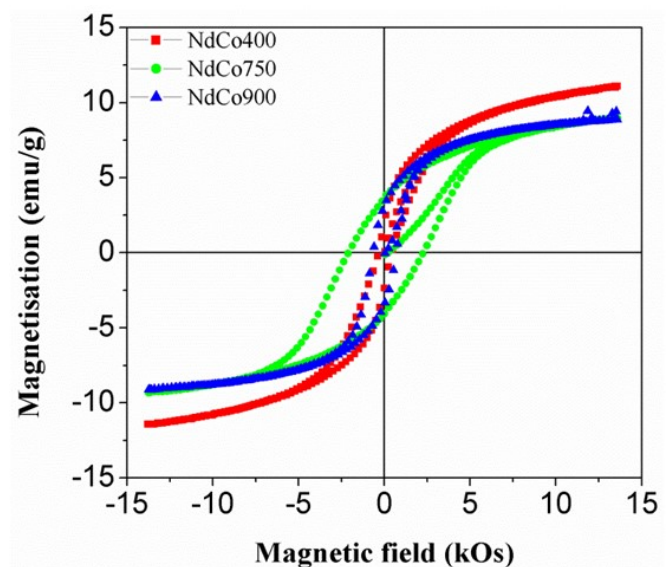


Figure 5. Room temperature magnetization hysteresis loops showing a decrease in saturation magnetization and increase in coercive field for powders annealed at 750 and 900°C .

not show any discernible variation with the changing T_A .

3.6 Photoluminescence

Figure 6 shows the room temperature emission of the powders NdCo400-900. The powders show T_A dependent photoluminescence (PL) spectral intensity. The spectra show a decrease in the PL intensity as T_A increased from 400 to 900°C for an excitation wavelength (λ_{ex}) of 390 nm. The decrease in the PL peak intensities here appear to reflect the increase in order as observed from the magnetization measurements as well as the PXRD patterns. Intensity appears to decrease as more ions are incorporated into the perovskite lattice and the structure takes shape. The decrease in peak intensity may be due to formation of multiple trap states in the perovskite lattice formed due to the substitution of the dopants into the lattice. This means that a longer time is required for the e^-h^+ recombination to occur for NdCo750 and even a longer time for NdCo900. This is good for photocatalysis.

3.7 Photocatalytic screening

The results of the Photocatalytic screening of NdCo400-900 on RhB dye are shown in Figure 7. The results show only slight activity for NdCo750 and NdCo 900 in the absence of H_2O_2 , while NdCo400 appears not to have a significant effect on the dye solution. In the presence of H_2O_2 , however, a significant impact is noticed in the Photocatalytic activities of the powders NdCo750 and NdCo900 with the latter being the most active (Figure 7). Organic and amorphous materials blocking the dye molecules from reaching the surface of the photo-

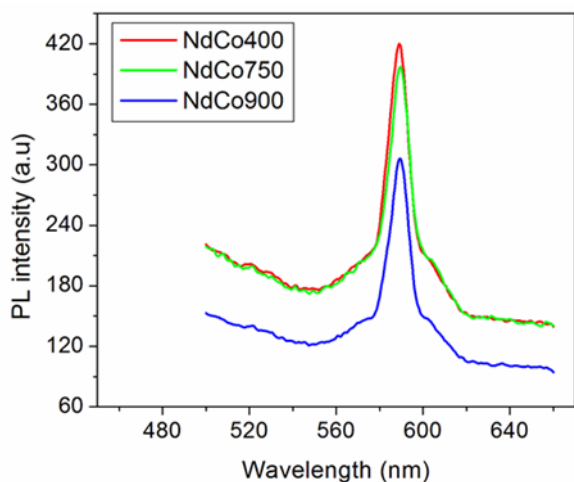


Figure 6. PL spectra showing the decrease in peak intensity as T_A is increased. e^-h^+ recombination may take longer for NdCo900.

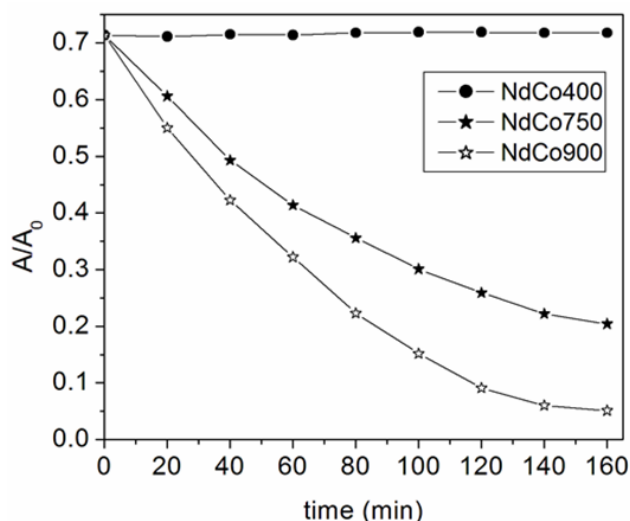


Figure 7. Photodegradation of RhB when irradiated with visible light for the photocatalysts NdCo400, 750 and 900 (1.5 g dm^{-3}) in the presence of H_2O_2 ($3.0 \times 10^{-5} \text{ mol dm}^{-3}$).

Table 3. Observed kinetics parameters for the photodegradation of RhB by 1.5 g dm^{-3} of photocatalysts (NdCo750-900) and $3.0 \times 10^{-5} \text{ mol dm}^{-3} H_2O_2$.

Sample	k_{obs}/min^{-1}	E/%
NdCo750 + H_2O_2	8.3×10^{-3}	79.6
NdCo900 + H_2O_2	1.6×10^{-2}	99.1

catalysts may explain the reason for the low or inactivity of powders annealed at $T_A = 400^\circ\text{C}$. The powders annealed at T_A 750 and 900°C , however, do not have such barriers and therefore were able to degrade the dye solution faster. The values of the observed rate constants and the calculated percent efficiency (E/%) (given by $E\% = ((A_0 - A)/A_0) \times 100$); where A_0 and A are the

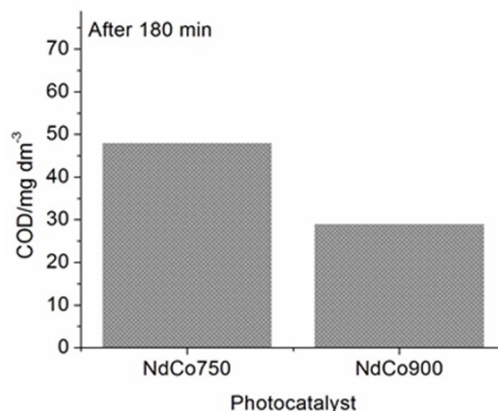


Figure 8. Analysis of the chemical oxygen demand (COD) for NdCo750 and NdCo900 after a period of 3 hours of photodegradation. The mineralization efficiency is 54 and 73 % respective-

initial and final absorbance of the dye solution respectively) are shown in Table 3. The NdCo750-900/H₂O₂ systems showed very high efficiency in decolourizing the RhB dye solution, suggesting that the materials can be excellent photocatalyst.

3.8 Mineralisation of the RhB dye

Figure 8 shows the COD results of the mineralisation of the dye solution by NdCo750 and NdCo900 after 180 min of Photocatalytic activity. The COD values obtained are 48 and 29 mg dm⁻³ of oxygen for NdCo750 and NdCo900, which represents an efficiency of 54 and 73 % mineralisation respectively. This shows that the photocatalyst can be used to effectively degrade organic pollutants and convert them to less harmful inorganic material.

4.0 CONCLUSIONS

Perovskite-like (Nd_{0.5}Bi_{0.2}Co_{0.2}Mn_{0.1})FeO_(3-δ) powders of crystallite size range from 17 to 33 nm were synthesized via a citric acid route. The PXRD results show the powders crystallized in a orthorhombic lattice with crystallite sizes increasing with T_A. The BET specific surface area was within the range of 12 to 5 nm. The saturation magnetization and the coercive fields both showed T_A dependence. The materials also showed improved magnetic properties with M_S values of up to 9.00 emu g⁻¹ and a H_C value of about 2181 Oe for NdCo750. The high coercive field value makes these materials good candidates for use in magnetic memory devices. photoluminescence activities within the visible region of the electromagnetic spectrum. The powders annealed at 750 and 900°C showed drastically improved Photocatalytic activity in the presence of H₂O₂ and up to 99% decolourization of RhB was achieved for NdCo900 and 73 % mineralization after 3 hours of exposure to visible light. The magnetisation of these materials at room temperature also means that they can easily be recovered after use as Photocatalyst. The author recommends a smaller incremental step be taken for the T_A so as to be able to determine the critical domain size for the material, also that these materials be further analysed so that other properties, such as charge transfer capacity be determined to ascertain its suitability for use in solid oxide fuel cells.

ACKNOWLEDGEMENTS

IA is grateful to the College of Agriculture, Engineering and Science at the University of KwaZulu-Natal for the award of a PhD bursary and a Doctoral Scholarship. The vibrating sample magnetometer used in this work was provided by the National Research Foundation of South Africa.

REFERENCES

- Chung, C. Y., Chang, Y. S., Chen, G. J., Chung, C. C. and Huang, T. W. (2008). Effects of bismuth doping on the dielectric properties of Ba(Fe_{0.5}Nb_{0.5})O₃ ceramic. *Solid State Communications*, 145(4): 212–217. <https://doi.org/10.1016/j.ssc.2007.10.035>.
- Ghasdi, M., Alamdari, H., Royer, S. and Adnot, A. (2011). Electrical and CO gas sensing properties of nanostructured La_{1-x}Ce_xCoO₃ perovskite prepared by activated reactive synthesis. *Sensors and Actuators, B: Chemical*, 156(1): 147–155. <https://doi.org/10.1016/j.snb.2011.04.003>.
- Herzer, G. (1990). Grain size dependence of coercivity and permeability in nanocrystalline ferromagnets. In *IEEE Transactions on Magnetics*, 26(5): 1397-1402.
- Inprasit, T., Wongkasemjit, S., Limthongkul, P. and Skinner, S. J. (2016). Synthesis and electrical property study of La₃Ni₂MO₉ (M=Nb and TA). *Materials Letters*, 162, 37–39. <https://doi.org/10.1016/j.matlet.2015.09.110>.
- Kanhere, P., Nisar, J., Tang, Y., Pathak, B., Ahuja, R., Zheng, J. and Chen, Z. (2012). Electronic structure, optical properties, and photocatalytic activities of LaFeO₃-NaTaO₃ solid solution. *Journal of Physical Chemistry C*, 116(43): 22767–22773. <https://doi.org/10.1021/jp307857h>.
- Khomchenko, V. A., Kiselev, D. A., Vieira, J. M., Jian, L., Kholkin, A. L., Lopes, A. M. L., Pogorelov, Y. G., Araujo, J. P. and Maglione, M. (2008). Effect of diamagnetic Ca, Sr, Pb, and Ba substitution on the crystal structure and multiferroic properties of the BiFeO₃ perovskite. *Journal of Applied Physics*, 103(2). <https://doi.org/10.1063/1.2836802>.
- Khomskii, D. I. (2006). Multiferroics: different ways to combine magnetism and ferroelectricity 1). *Journal of Magnet and Magnetic Materials*, 306, 1–8. www.elsevier.com/locate/jmmm.
- Lantto, V., Saukko, S., Toan, N. N., Reyes, L. F. and Granqvist, C. G. (2004). Gas Sensing with Perovskite-like Oxides Having ABO₃ and BO₃ Structures. *Journal of Electroceramics*, 13: 721–726.
- Lerdprom, W., Li, C., Jayaseelan, D. D., Skinner, S. J. and Lee, W. E. (2017). Temperature dependence of electrical conductivity of a green porcelain mixture. *Journal of the European Ceramic Society*, 37(1): 343–349. <https://doi.org/10.1016/j.jeurceramsoc.2016.08.019>.
- Li, M., Ning, M., Ma, Y., Wu, Q. and Ong, C. K. (2007). Room temperature ferroelectric, ferromagnetic and magnetoelectric properties of Ba-doped BiFeO₃ thin films. *Journal of Physics D: Applied Physics*, 40(6): 1603–1607. <https://doi.org/10.1088/0022-3727/40/6/002>.
- Liang, Y. Q., Di, N. L. and Cheng, Z. H. (2005). Charge-disproportionation-induced magnetic glassy behavior in La_{0.5}Ca_{0.5}FeO_{3-δ}. *Physical Review B - Condensed Matter and Materials Physics*, 72(13): <https://doi.org/10.1103/PhysRevB.72.134416>.
- Lu, Z., Chen, L., Tang, Y. and Li, Y. (2005). Preparation and luminescence properties of Eu³⁺-doped MSnO₃ (M= Ca, Sr and Ba) perovskite materials. *Journal of Alloys and Compounds*, 387(1–2): L1–L4.
- Machida, M., Yabunaka, J. I. and Kijima, T. (2000). Synthe-

- sis and photocatalytic property of layered perovskite tantalates, $\text{RbLnTa}_2\text{O}_7$ (Ln = La, Pr, Nd, and Sm). *Chemistry of Materials*, 12(3): 812–817. <https://doi.org/10.1021/cm990577j>.
- Maguire, E., Gharbage, B., Marques, F. M. B. and Labrincha, J. A. (2000). Cathode materials for intermediate temperature SOFCs. In *Solid State Ionics* (Vol. 127). www.elsevier.com/locate/ssi.
- Nforna E. A, Tsobnang P. K, Fomekong R. L, Tedjieukeng H. M. K, Lambi J. N. and Ghogomu J. N. (2021). Effect of B-site Co substitution on the structure and magnetic properties of nanocrystalline neodymium orthoferrite synthesized by auto-combustion. *Royal Society Open access Science*. 7: 201883-201896. <https://doi.org/10.1098/rsos.201883>.
- Nguyen, T. A.; Pham, T. L.; Mittova, I. Y.; Mittova, V. O.; Nguyen, T. L. T.; Nguyen, H. V. and Bui, V.X. (2021). Co-Doped NdFeO_3 Nanoparticles: Synthesis, Optical, and Magnetic Properties Study. *Nanomaterials* 11: (04). 937. <https://doi.org/10.3390/nano11040937>.
- Paik, D.-S., Park, S.-E., Shrout, T. R. and Hackenberger, W. (1999). Dielectric and piezoelectric properties of perovskite materials at cryogenic temperatures. *Journal of Materials Science*, 34(3): 469-473.
- Peel, M. D., Ashbrook, S. E. and Lightfoot, P. (2013). Unusual phase behavior in the piezoelectric perovskite system, $\text{Li}_x\text{Na}_{1-x}\text{NbO}_3$. *Inorganic Chemistry*, 52(15): 8872–8880. <https://doi.org/10.1021/ic401061t>.
- Ramajo, L., Castro, M., del Campo, A., Fernandez, J. F. and Rubio-Marcos, F. (2014). Influence of B-site compositional homogeneity on properties of $(\text{K}_{0.44}\text{Na}_{0.52}\text{Li}_{0.04})(\text{Nb}_{0.86}\text{Ta}_{0.10}\text{Sb}_{0.04})\text{O}_3$ -based piezoelectric ceramics. *Journal of the European Ceramic Society*, 34(10): 2249–2257. <https://doi.org/10.1016/j.jeurceramsoc.2014.02.002>.
- Shalini, T., Vijayakumar, P. and Kumar, J. (2020). Studies on structural and magnetic properties of NdFeO_3 single crystals grown by optical floating zone technique. *Bulletin of Materials Science*, 43(1): 1-7.
- Sing, K. S. W., Everett, D. H., Haul, R. A. W., Moscou, L., Pierotti, R. A., Rouquerol, J. and Siemieniowska, T. (1985). Reporting physisorption data for gas/solid systems with special reference to the determination of surface area and porosity (Recommendations 1984). *Pure Applied Chemistry* 57(4): 603–619.
- Skinner, S. J. (2001). Recent advances in Perovskite-type materials for solid oxide fuel cell cathodes. *International Journal of Inorganic Materials*, 3: 113–121. [https://doi.org/10.1016/S1466-6049\(01\)0004-6](https://doi.org/10.1016/S1466-6049(01)0004-6).
- Tang, J., Zhu, M., Zhong, T., Hou, Y., Wang, H. and Yan, H. (2007). Synthesis of fine $\text{Pb}(\text{Fe}_{0.5}\text{Nb}_{0.5})\text{O}_3$ perovskite powders by coprecipitation method. *Materials Chemistry and Physics*, 101(2–3): 475–479. <https://doi.org/10.1016/j.matchemphys.2006.08.006>.
- Wang, L. Y., Wang, D. H., Huang, H. B., Han, Z. D., Cao, Q. Q., Gu, B. X. and Du, Y. W. (2009). The magnetic properties of polycrystalline $\text{Bi}_{1-x}\text{Sr}_x\text{FeO}_3$ ceramics. *Journal of Alloys and Compounds*, 469(1–2): 1–3. <https://doi.org/10.1016/j.jallcom.2008.01.095>.
- Williams I. D. (2001). *Environmental Chemistry; A Modular Approach* (1 edition). John Wiley and Sons. <http://eu.wiley.com/WileyCDA/WileyTitle/productCd-0471489417.html>.
- Yu, K., Yang, S., Liu, C., Chen, H., Li, H., Sun, C. and Boyd, S. A. (2012). Degradation of organic dyes via bismuth silver oxide initiated direct oxidation coupled with sodium bismuthate based visible light photocatalysis. *Environmental Science and Technology*, 46(13): 7318–7326. <https://doi.org/10.1021/es3001954>.
- Zhang, H., Fu, X., Niu, S. and Xin, Q. (2008). Synthesis and photoluminescence properties of Eu^{3+} -doped AZrO_3 (A = Ca, Sr, Ba) perovskite. *Journal of Alloys and Compounds*, 459(1–2): 103–106. <https://doi.org/10.1016/j.jallcom.2007.04.259>.
- Zhu, J., Li, H., Zhong, L., Xiao, P., Xu, X., Yang, X., Zhao, Z. and Li, J. (2014). Perovskite oxides: Preparation, characterizations, and applications in heterogeneous catalysis. *ACS Catalysis*, 4(9): 2917–2940. <https://doi.org/10.1021/cs500606g>.